Spatiotemporally resolved characteristics of a gliding arc discharge in a turbulent air flow at atmospheric pressure

Zhu, Jiajian; Gao, Jinlong; Ehn, Andreas; Aldén, Marcus; Larsson, Anders; Kusano, Yukihiro; Li, Zhongshan

Published in:
Physics of Plasmas

DOI:
10.1063/1.4974266

2017

Title page:

Spatiotemporally resolved characteristics of a gliding arc discharge in a turbulent air flow at atmospheric pressure

Jiajian Zhu[1,2], Jinlong Gao[2], Andreas Ehn[2], Marcus Aldén[2], Anders Larsson[3], Yukihiro Kusano[4] and Zhongshan Li[2*]

[1]Science and Technology on Scramjet Laboratory, National University of Defense Technology, Changsha 410073, China

[2]Division of Combustion Physics, Lund University, P.O. Box 118, S-221 00 Lund, Sweden

[3]Swedish Defense Research Agency, SE-164 90 Stockholm, Sweden

[4]Department of Wind Energy, Section for Composites and Materials Mechanics, Technical University of Denmark, Risø Campus, Frederiksborgvej 399, DK-4000 Roskilde, Denmark

[*]Corresponding author: zhongshan.li@forbrf.lth.se

This is the peer reviewed version of the following article: [J.J. Zhu, J. Gao, A. Ehn, M. Aldén, Z.S. Li, A. Larsson and Y. Kusano, '*Spatiotemporally resolved characteristics of a gliding arc discharge in a turbulent air flow at atmospheric pressure*', **Physics of Plasma 24**, 013514 **(2017)**.], which has been published in final form at: https://aip.scitation.org/doi/10.1063/1.4974266.

Spatiotemporally resolved characteristics of a gliding arc discharge in a turbulent air flow at atmospheric pressure

Jiajian Zhu[1,2], Jinlong Gao[2], Andreas Ehn[2], Marcus Aldén[2], Anders Larsson[3], Yukihiro Kusano[4] and Zhongshan Li[2*]

[1]Science and Technology on Scramjet Laboratory, National University of Defense Technology, Changsha 410073, China

[2]Division of Combustion Physics, Lund University, P.O. Box 118, S-221 00 Lund, Sweden

[3]Swedish Defense Research Agency, SE-164 90 Stockholm, Sweden

[4]Department of Wind Energy, Section for Composites and Materials Mechanics, Technical University of Denmark, Risø Campus, Frederiksborgvej 399, DK-4000 Roskilde, Denmark

[*]Corresponding author: zhongshan.li@forbrf.lth.se

A gliding arc discharge was generated in a turbulent air flow at atmospheric pressure driven by a 35 kHz alternating current (AC) electric power. The spatiotemporally resolved characteristics of the gliding arc discharge, including glow-type discharges, spark-type discharges, short-cutting events and transitions among the different types of discharges, were investigated using simultaneously optical and electrical diagnostics. The glow-type discharge shows sinusoidal-like voltage and current waveforms with a peak current of hundreds of *mA*. The frequency of the emission intensity variation of the glow-type discharge is the same as that of the electronic power dissipated in the plasma column. The glow-type discharge can transfer into a spark discharge characterized by a sharp peak current of several *A* and a sudden increase of the brightness of the plasma column. Transitions from spark-type discharges to glow-type discharges have been observed. Short-cutting events were also observed as the intermediate states formed during the spark-glow transition. Three different types of short-cutting events have been identified to generate new current paths between two plasma channel segments, between two electrodes, and between the channel segment and one of the electrodes, respectively. The short-cut upper part of the plasma column that was found to have no current passing through can be detected several hundreds of microseconds after the short-cutting event. The voltage recovery rate, the period of AC voltage-driving signal, the flow rates and the rated input powers were found to play an important role in affecting the transitions among the different types of discharges.

I. INTRODUCTION

Non-thermal plasmas with high electron temperature and low gas temperature consume less energy on gas heating, and are efficient in producing reactive species. A gliding arc discharge can be used to generate non-thermal plasmas at atmospheric pressure[1, 2], and has been used for numerous applications, such as pollution control[3-7], combustion enhancement[8, 9], and surface treatment[10-13]. The optimization of gliding arc discharges for different applications has attracted increasing interest in non-intrusive optical diagnostics and electrical measurements.

Many optical diagnostic tools have been used to investigate gliding arc discharges, including planar laser-induced fluorescence[14, 15], optical emission spectroscopy[16-21], photography by regular digital cameras[22-24], CCD cameras[25, 26] and high-speed cameras[27-32]. High-speed photography with exposure times of a few microseconds are able to reveal the transient structure of a gliding arc discharge, and capture the motions and the instantaneous length of the plasma column and cycles of ignition-extension-extinction[14, 15]. Electrical measurements of the gliding arc discharges often focus on recording voltage and current, which are used to estimate the impedance and power dissipated in the plasma column[33-39], and distinguish different types of discharge phenomena observed in the gliding arc discharge[22, 23]. Simultaneous high-speed photography and electrical measurements allow direct observations of the dynamics of the plasma column synchronized with the instantaneous electric parameters[29, 30, 40, 41]. The simultaneous observations are useful for gaining a better understanding of detailed spatiotemporally resolved characteristics of the gliding arc discharge, especially for that driven by

a kHz alternating current (AC) and operated in a turbulent flow.

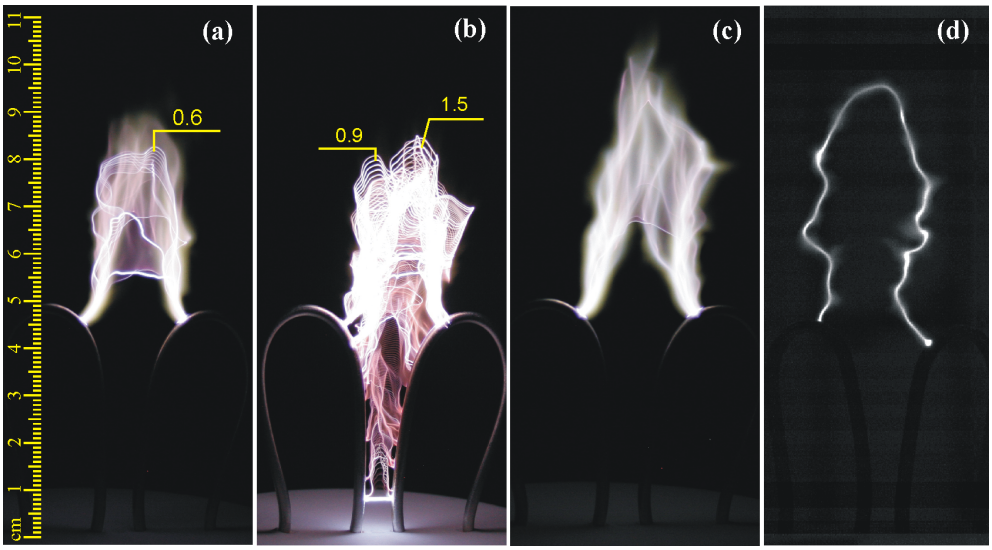

FIG. 1. *Photos of a 35 kHz gliding arc discharge operated at different input powers and air flow rates between the electrodes: (a) 600 W and 17.5 SLM (standard liter per minute); (b) 600 W and 42 SLM; (c) 800 W and 17.5 SLM; (d) Instantaneous image of a typical plasma column. The photos in (a), (b), (c) were recorded by a digital camera with an exposure time of 1/60 s while that in (d) was captured by a high-speed camera with an exposure time of 16.25 μs. Typical distances between two bright plasma columns are marked in (a) and (b) in units of millimeter.*

Our previous studies have shown that a kHz AC gliding arc discharge in a turbulent flow are both temporally and spatially complex[14, 15, 28]. Comprehensive diagnostics of a kHz AC gliding arc discharge in a turbulent air have shown that a sustained diffusive discharge can be achieved in a large volume by matching air flow rate with the AC power[27]. However, more operation modes of the gliding arc discharge were found, as shown in figure 1, due to the complex interactions between the turbulent flow and highly dynamic AC discharge. Systematic investigations are required to reveal the governing mechanisms. Figure 1 shows photos of the gliding arc discharge recorded at different input powers and flow rates. Alternately bright and dark fringes are observed in figure 1 (a) and (b). However, on the other hand, the alternately bright and dark fringes are hardly visible, and a more diffusive discharge is observed in figure 1(c), for which a higher electric power is used.

The presented work attempts to clarify these distinctive features of the gliding arc discharge and study the spatiotemporally resolved characteristics using simultaneously high-speed observations and electrical measurements. The goal is to achieve an optimized operation of the gliding arc discharge and gain a better understanding of mechanisms governing of gas discharges in a turbulent flow at atmospheric pressure.

II. EXPEIMENTAL SETUP

Figure 2 shows a schematic of the gliding arc discharge system as well as the optical and electrical measurement setup. The gliding arc discharge is ignited at the narrowest gap (7 mm) between two diverging electrodes (see figure 1). The hollow tubular electrodes are water-cooled stainless steel tubes with an outer diameter of 3 mm. An air-flow controlled by a mass flow controller is used to blow the plasma column upwards through a nozzle of 3 mm diameter. A high-voltage transformer and a power supply (Generator 9030E, SOFTAL Electronic GmbH, Germany) with adjustable output electric powers are employed to generate a 35 kHz AC high voltage. A similar gliding arc discharge system was described in our previous works[12, 14, 15, 27, 28].

Evolution of the plasma column was recorded using a high-speed camera (Fastcam SA-X2, Photron) equipped with an objective lens (Micro-Nikkor 105 mm, f/2.8). The high-speed camera was operated at a frame

rate of 50 or 480 kHz. The 50 kHz operation enables capturing the motions of whole plasma columns with a resolution of 768×328 pixels, whereas the 480 kHz operation with a resolution of 128×48 pixels enables the resolution of the phase influence of the 35 kHz AC voltage-driving signal on the discharge characteristics.

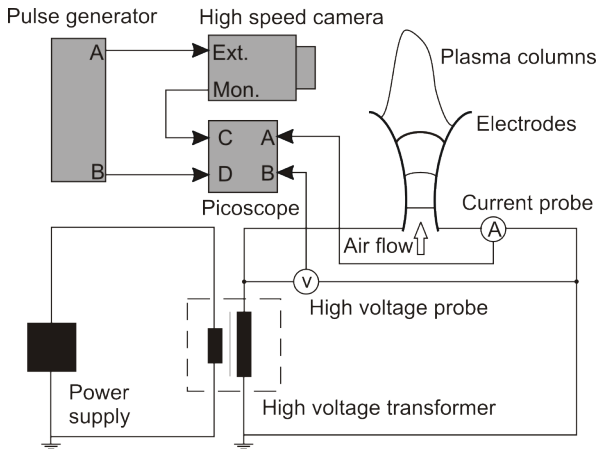

FIG. 2. *Schematic of the experimental setup for simultaneously optical and electrical measurement of the AC gliding arc discharge.*

The voltage and current were measured by a high-voltage probe (P6015A, Tektronix) and a current monitor (model 6585, Pearson Electronics), respectively. Both the voltage and current were recorded by a four-channel oscilloscope (PicoScope 4424). A pulse generator (BNC 575) was employed to synchronize the acquisition of the plasma column images and the voltage and current waveforms. The gate signal of the high-speed camera and the instantaneous voltage and current waveforms were recorded by the oscilloscope simultaneously.

III. SPATIAL AND TEMPORAL FEATURES OF DIFFERENT TYPES OF DISCHARGES

Figure 3 shows voltage and current waveforms of a gliding arc discharge with 600 W rated AC input power and 17.5 SLM air flow rate during a 100 ms time span, which corresponds to the operating condition shown in figure 1(a). The voltage exhibits a sawtooth-like envelope with the largest peak voltage at around 20 kV, whereas the current approximately peaks at hundreds of mA with frequently occurring spikes of around 10 A. Several zoomed-in parts of the waveforms in figure 3 are described below together with discussion about spatial and temporal features of different types of discharges.

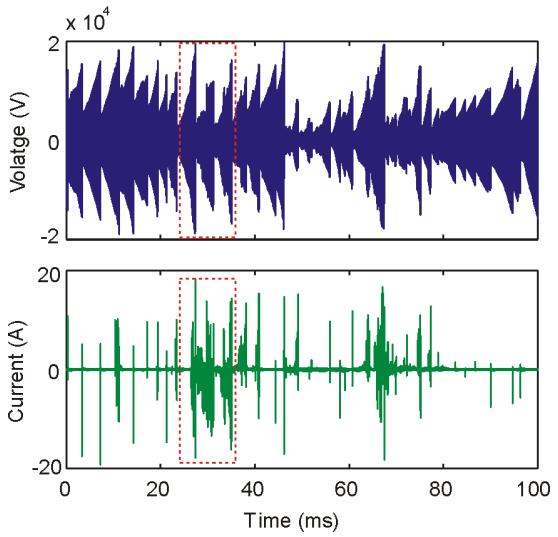

FIG. 3. *Voltage and current waveforms of a gliding arc discharge operated at 600 W and 17.5 SLM. The rectangles mark the parts shown in figure 13.*

A. Glow-type discharges (GD)

A zoomed-in waveform of figure 3 at around 24.8 ms is shown in figure 4(a), in which a typical glow-type discharge characterized by the peak current of hundreds of mA is observed. The gated exposure times of the high-speed camera are labeled in figure 4(a) with red dashed lines. At the glow-type discharge, the voltage and current show sinusoidal-like waveforms. Typical values for the peak voltage and current are about 5 kV and 0.2 A, respectively. Figure 4(b) shows the sequential images of plasma columns, which anchor above the electrodes of about 5 cm long. The length was evaluated using 2D images, which may underestimate the length of plasma columns by up to 25%[28]. The emission intensity of different plasma columns in figure 4(b) is at a similar level since the relatively long exposure time (16.25 μs) is unable to resolve the phase of the AC driving signal of 28 μs.

The glow-type discharge can be sustained for about 2 milliseconds in this specific case. The voltage and the current varied with the length of the plasma columns extended by the external air flow. Figure 5(a) shows the voltage-current waveforms of the glow-type discharge at around 26 ms, which is 1.2 ms after that illustrated in figure 4(a). Compared to figure 4(a), the peak voltage in figure 5(a) increases to 9 kV and the peak current decreases to 0.1 A. In addition, the length of the plasma column increased to approximately 10 cm.

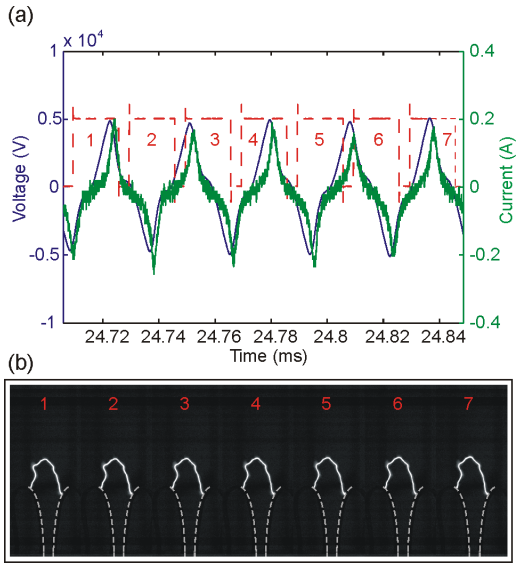

FIG. 4. *Glow-type discharge at around 24.8 ms. (a) Voltage, current and camera gates; (b) Sequential images of plasma columns recorded over camera gate labeled in (a). The images are captured every 20 μs with an exposure time of 16.25 μs. The dashed lines in (b) illustrate the positions of the two electrodes.*

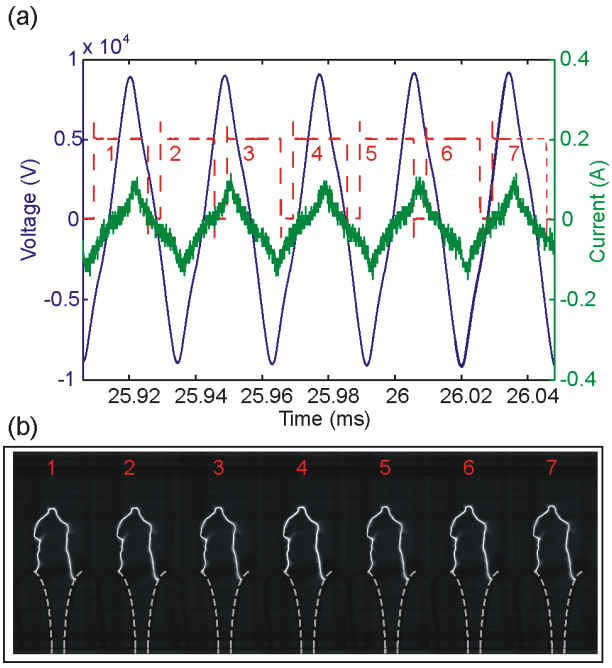

FIG. 5. *Glow-type discharge at around 26 ms. (a) Voltage, current and camera gates; (b) Sequential images of plasma columns recorded over each camera gate as labeled in (a).*

Figure 6(a) shows extension of a typical glow-type discharge, whereas figure 6(b) summarizes evolution of the length, the peak voltage and the peak current of the glow-type discharge over 2 ms time span. As the glow-type discharge glides upwards over the 2 ms time span, the voltage of the plasma column almost linearly increases with the increasing length of plasma columns while the peak current decreases from 0.3 to 0.1 A.

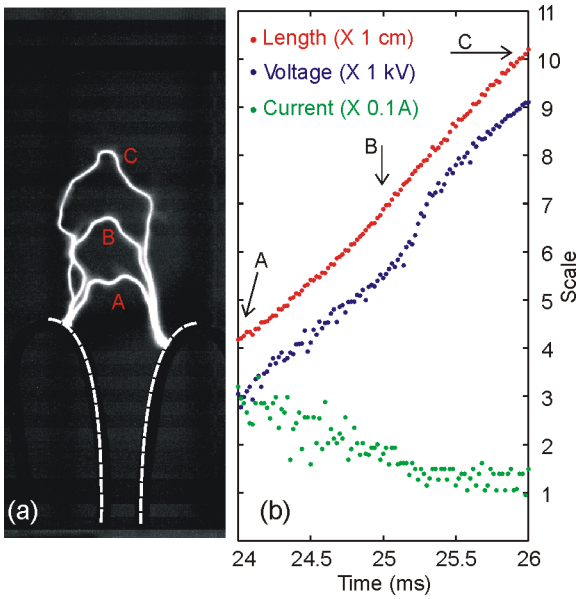

FIG. 6. *(a) Extension of a typical glow-type discharge; (b) Evolution of the length, the peak voltage, the peak current of the glow-type discharge over 2 ms time span. The occurrence time of the plasma columns, namely A, B and C, are marked in (b). The corresponding scales for the length (cm), the peak voltage (kV), and the peak current (0.1A) are labeled in (b). A high-speed movie that shows the evolution of the plasma column over this period is available in the supplement. "(Multimedia view)"*

B. Spark-type discharges (SD)

Spark-type discharges are recognized by current spikes of several to tens of amperes, displayed in figure 3. Figure 7 illustrates that the spark-discharge can be observed with a time interval of 14 μs, corresponding to a half period of the AC voltage-driving signal. The sinusoidal-like waveform found in the glow-type discharge is significantly deformed here. Some periodically occurring current spikes with a magnitude of about 4 *A* are recognized. The current spike lasts only for hundreds of nanoseconds or shorter, and then the current is reduced to about tens of mA, as shown in the insert of figure 7(a). As soon as the current spike occurs, the voltage abruptly decreases. After the rapid drop, the

voltage gradually recovers again to about 5 kV, initiating another current spike. The camera gate illustrated in figure 7(a) captures at least one of the current spikes, in a 4-cm-long spark-type plasma column as displayed in figure 7(b).

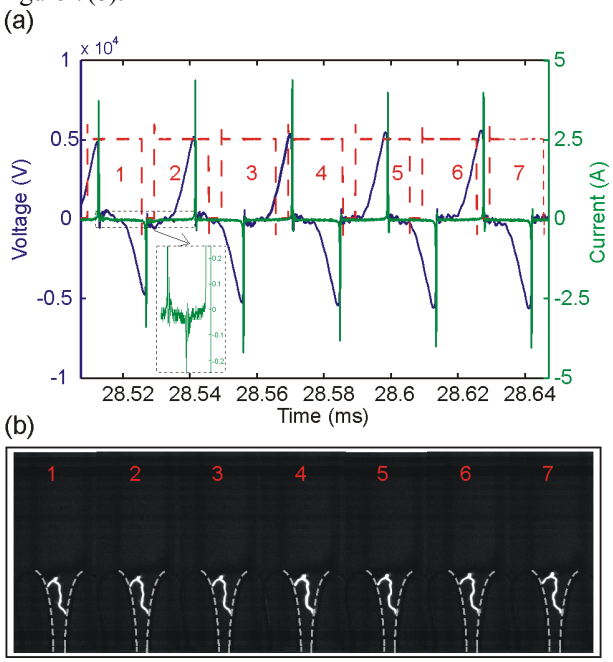

FIG. 7. *Spark-type discharge with a time interval of 14 μs. (a) Voltage, current and camera gates; (b) Sequential images of plasma columns recorded over each camera gate as labeled in (a).The current with small magnitudes is plotted as an insert in (a) for the period marked by the dashed rectangles in (a).*

It is also found that the time span between two sequential spark-type discharges increases with the length of the plasma column. The time span can be several times as large as the half period of the AC driving power supply. Figure 8 shows an example of the current spikes with time intervals of 70 and 84 μs. Whenever there is a current spike, the corresponding voltage significantly decreases, and then the peak voltage gradually increases until a new current spike occurs. Figure 9 shows the spark-type discharge with a time interval of 84 μs. Compared to the spark-type discharges with smaller time intervals in figure 7, the spark-type discharges here show longer plasma columns and higher peak voltage. For the spark-type discharge, a current

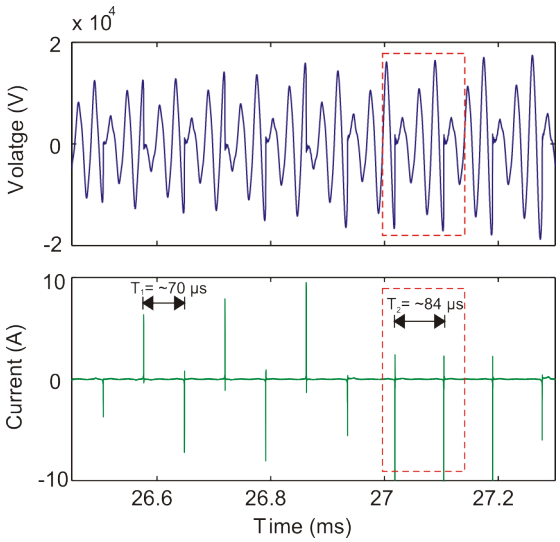

FIG. 8. *Voltage and current waveforms of spark-type discharges. The typical time intervals (70 and 84 μs) between two sequential current spikes are labeled. The waveforms marked by rectangles are zoomed in figure 9(a).*

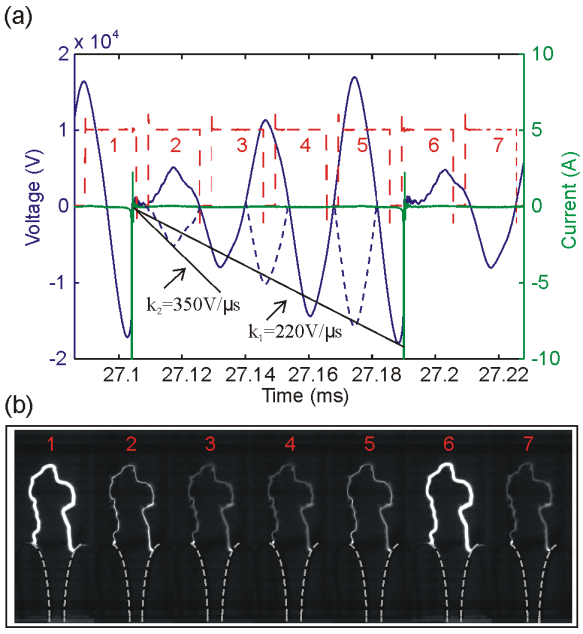

FIG. 9. *Spark-type discharge with a time interval of 84 μs. (a) Voltage, current and camera gates; (b) Sequential images of plasma columns. The range of the voltage recovery rate after an abrupt voltage drop is shown in (a) as the slope of the labeled curves.*

spike is observed together with an abrupt drop of the peak voltage and subsequent voltage recovery. A new current spike as a breakdown through the plasma column will ignite as soon as the peak voltage raided up to a value related the length of the plasma column. The

voltage recovery rate is revealed from the labeled slope in figure 9(a), namely 220 - 350 V/μs. It should be noted that transitions between the glow-type discharges and spark-discharges can be observed in figure 9. Between the two spark-type discharges characterized by a sudden increase of the brightness of the plasma column, glow-type discharges can be usually seen. The time interval of the spark-glow transitions is 84 μs here.

C. Short-cutting events (Sc)

Short-cutting events in the plasma column significantly affect the evolution and elongation of the gliding arc discharge. The short-cutting events include short-cutting phenomena between two channel segments, and between electrodes, as well as between the channel segment and one of the electrodes.

C1. Short-cutting events between channel segments (Sc1)

In short-cutting events between two channel segments, a new conductive pathway is formed, shortcutting the upper part of the plasma column[14, 15, 27]. Once the short-cutting event takes place, an abrupt current peak of about 10 *A* occurs, resulting in a bright plasma column and an afterglow upper part as shown in figure 10. After hundreds of nanoseconds [27], the current is reduced to hundreds of mA and the transition from spark-type to glow-type discharge is formed. However, another current peak (1 *A*) is recognized after tens of microseconds, which corresponds to the plasma column shown in the fifth image of figure 10(b).

C2. Short-cutting events between electrodes (Sc2)

Figure 11 shows short-cutting events between electrodes where a re-ignition of a new plasma column can be seen. A current peak of 20 *A* and a significant decrease of voltage magnitude can be found in the re-ignition event. The breakdown voltage is about 20 kV, and the narrowest gap between the electrodes is about 7 mm. It suggests that the electric field strength for the breakdown is about 3 MV/m. Note that the afterglow still exists for hundreds of microseconds after the new ignition. Previous investigations have shown that the decay rate of the afterglow is affected by the gas flow rate [15].

C3. Short-cutting events between the channel segment and the electrode (Sc3)

When the gliding arc discharge is ignited at the narrowest gap between the two electrodes, the plasma column is normally extended by the gas flow, and it continuously moves in an upward direction along the electrodes. However, sometimes the anchor point of the plasma column on the electrode jumps from one place to another due to a short-cutting event between the channel segment and the electrode. Note that both the upwards and backwards jumps of the anchor point are observed in the turbulent gliding arc discharge. Such an event is shown in figure 12. A peak current was observed in the second gate in figure 12(a), and the corresponding short-cutting event between the channel segment and the electrode is marked in figure 12(b). The reason for the jump may due to a potential difference between the point A on the plasma column and the point B on the electrode. The potential difference is approximately 1000 V, which makes it possible to generate the short-cutting event between the point A on the plasma column and the point C on the electrode and form the jump of the spot from point B to point C. Similar findings were previously reported both in the experiment [26] and the 2D model[42].

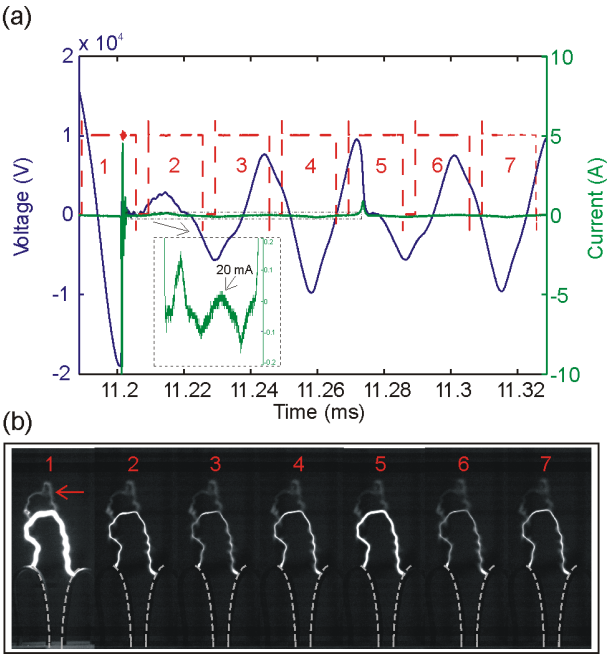

FIG. 10. *Short-cutting events between two channel segments. (a) Voltage, current and camera gates; (b) Sequential images of plasma columns recorded over each camera gate as labeled in (a). The current in between spikes is plotted as an insert in (a) as marked by the*

dashed rectangles. The afterglow of short-cut upper part of the plasma column is marked in (b) by an arrow.

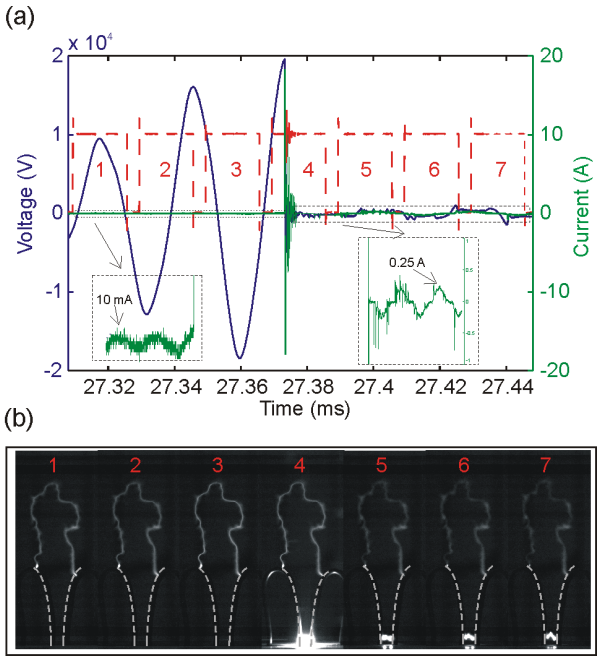

FIG. 11. *Short-cutting events between electrodes. (a) Voltage, current and camera gates; (b) Sequential images of plasma columns recorded over each camera gate as labeled in (a). The detail of the weak current plotted as inserts in (a) shown by the dashed rectangles.*

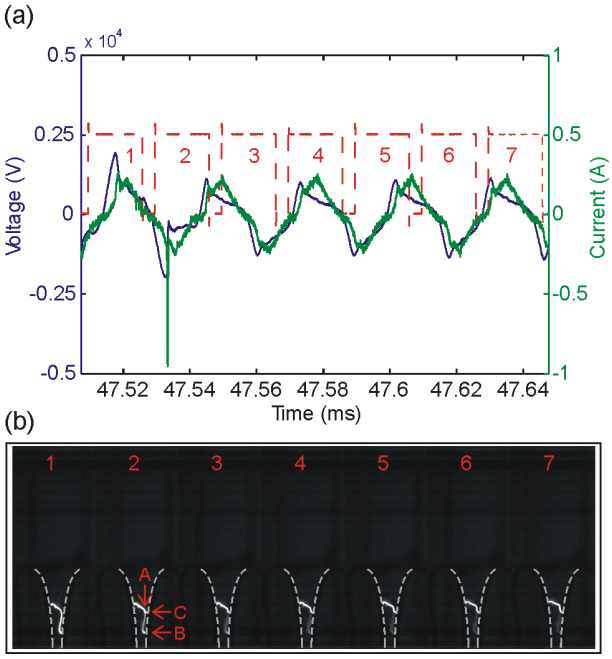

FIG. 12. *Short-cutting events between the channel segment and the electrode. (a) Voltage, current and camera gates; (b) Sequential images of plasma columns recorded over each camera gate as labeled in (a)*

.IV. TRANSITIONS AMONG DIFFERENT TYPES OF DISCHARGES

A. Dynamic transition processes

Dynamic transition processes of the gliding arc discharge can be observed in figure 13 that is the zoomed-in voltage and current waveform marked in figure 3.

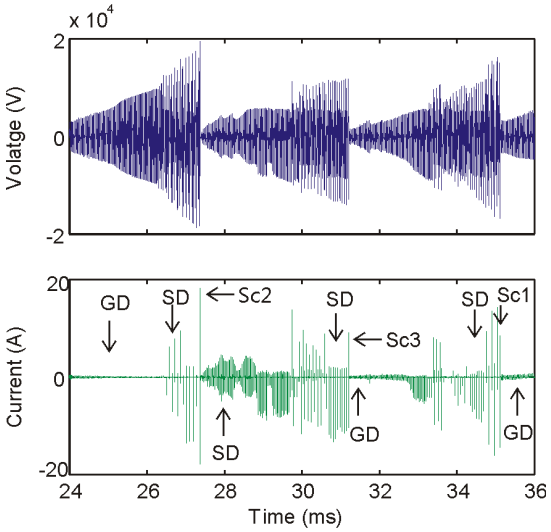

FIG. 13. *Zoomed-in voltage and current waveforms marked in figure 3, showing the dynamic transition processes of different types of discharges. Typical examples of discharge phenomena are labeled (GD: glow-type discharges; SD: spark-type discharges; Sc1: short-cutting between two channel segments; Sc2: short-cutting between two electrodes or re-ignition; Sc3: short-cutting between a channel segment and an electrode). The movie of the plasma column recorded simultaneously with the voltage and current waveforms is also available in the supplement. "(Multimedia view)"*

Examples of typical discharge phenomena mentioned above are labeled in the figure. The largest voltage peak (about 20 kV) are resulted from a short-cutting event between two electrodes (Sc2) or re-ignition. After the re-ignition of the gliding arc discharge, the spark-type discharge (SD) with the shortest time interval (14 μs) is observed between the two electrodes. Between two sequential spark-type discharges, glow-type discharges can be usually seen. As the plasma column

glides along the electrodes, transitions from spark-type discharges or glow-type discharges to short-cutting events between the channel segment and the electrode (Sc3) are occasionally identified. After the spark-type plasma column is extended upwards with a longer length, the spark-type discharges with a time interval of 70 μs or 84 μs always end up with short-cutting events (Sc1, Sc2 or Sc3) and then transfer to glow-type discharges (GD), as labeled in figure 13. The detailed transition processes of the gliding arc discharge can be clearly seen in the supplementary video. *"(Multimedia view)"*

The dynamic transition processes between glow-type discharges and spark-discharges can be shown in figure 14. Figure 14(a) demonstrates phase-resolved emission intensities of plasma columns at the spark-glow transitions and the sustained glow-type discharge. Each data point in figure 14(a) represents the emission intensity of a plasma column recorded by the high-speed camera at a 480 kHz frame rate. The transient intensity peak at the curve of the spark-glow transitions indicates the occurrence of a spark-type discharge. When the spark-discharge is generated, it immediately transfers itself to glow-type discharge. The spark-glow transitions are periodically observed with a time interval of 28 μs. It should be noted that spark-glow transitions could be also observed with other periods that are normally several times more than one-half cycle of the AC voltage-driving signal. The smallest period of the spark-glow transitions is 14 μs (cf. figure 7)whereas the largest period observed is up to 84 μs (cf. figure 9). The gliding arc discharge can also be operated as a sustained glow-type discharge, as seen in figure 14(a). The emission intensity of the glow-type discharge is always fluctuating at a time interval of 14μs that is the same as one-half cycle of the AC voltage-driving signal. Figure 14(b) shows the power dissipated in the plasma columns calculated from the voltage and current waveforms. Compared the results in figure 14(b) with figure 14(a), it can be concluded that the variation frequency of the emission intensity is the same as that of the electronic power dissipated in the plasma column for both the spark-glow transitions and the sustained glow-type discharge. It means that the input power to the gliding arc discharge plays a key role in affecting the transitions between spark-type discharges and glow-type discharges.

Short-cutting events are the intermediate discharges produced during the spark-glow transitions. As shown in figure 11, the short-cutting event between the two electrodes leads to a glow-to-spark transition. On the other hand, the short-cutting events between the channel

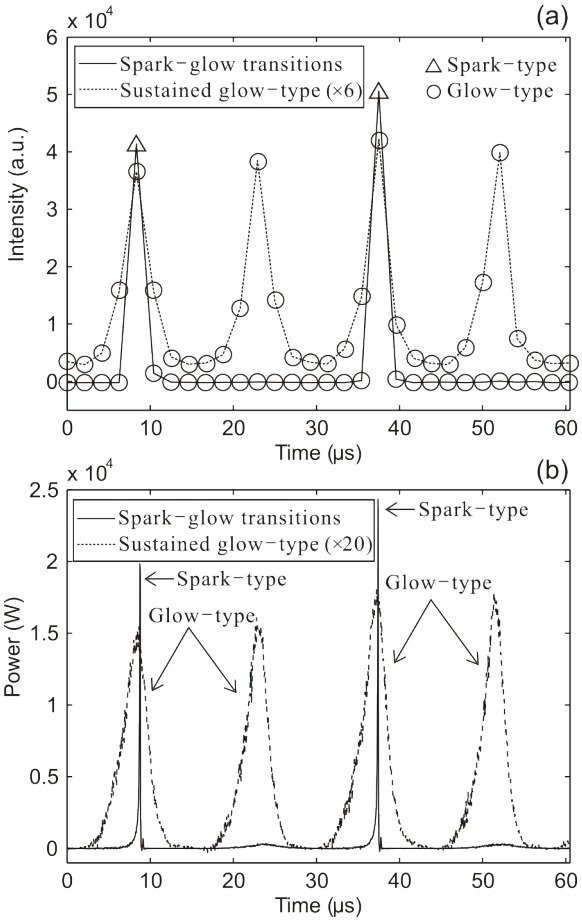

FIG. 14. *(a) Emission intensity of the spark-glow transitions and the sustained glow-type discharge recorded by a 480 kHz high-speed camera; (b) Electric power of the spark-glow transitions and the sustained glow-type discharge calculated from recorded current and voltage waveforms.*

segments can also generate a spark-to-glow transition which is observed in figure 10. Figure 15 shows emission intensities of a plasma column during a spark-to-glow transition induced by a short-cutting event. The emission intensities of the upper and lower parts of the plasma columns after the short-cutting event are integrated, as labeled in figure 15 by two rectangles. The emission intensity of the low part decreases immediately after the short-cutting event and create a spark-to-glow transition. After the spark-to-glow transition, the emission intensity is fluctuating and a sustained glow-

type discharge is formed. However, it is obvious that the emission intensity of the upper part gradually decreases after the short-cutting events. It is concluded from figure 14 that the intensity of the plasma column should fluctuate if the alternating current is passing through the plasma column. In other words, it suggests that there is no current in the upper part after the shorting-cutting event occurs. The visible emission in the upper part may come from the de-excitation of long-lived species that can be detected several hundreds of microseconds after the short-cutting event.

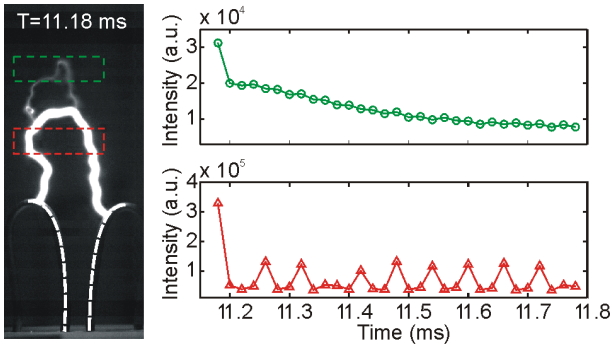

FIG. 15. *Emission intensity of plasma columns during a spark-to-glow transition induced by a short-cutting event. The upper (circles) and lower (triangles) part of the short-cutting plasma column shows a decaying and fluctuating trend, respectively.*

B. Effect of flow rates

Figure 16 shows the voltage and current waveforms at 600 W and 42 SLM. This has the same operating condition that is displayed in figure 1(b). Typical examples of discharge phenomena are denoted in the figure. Compared to the waveforms that are captured with a lower flow rate of 17.5 SLM, shown in figure 13, more current spikes are observed in figure 16, suggesting that the more frequent transitions among different types of discharges at the higher flow rate.

The flow rate has a significant impact on the discharge mainly due to effects of turbulence[15, 23]. The Reynolds number and the Kolmogorov length (the size of the smallest turbulent eddies) of the turbulent flows used in the experiment are calculated and listed in Table. 1. With increasing flow rates, the Kolmogorov length (the smallest length of turbulence eddies) becomes smaller[15, 23]. The eddies or vortices of turbulence are more likely to penetrate into the plasma column and transport the heat and mass to the surrounding air, which quickly cool and quench the plasma column, resulting in more re-ignitions and spark discharges. In addition, the occurrence of the spark-type discharge may also be due to the interaction between the residual species and turbulence. Residual long-lived metastable species produced in the previous plasma channel may promote the formation of the next spark-type discharge. Furthermore, the turbulent air flow twists and wrinkles the plasma column and transports long-lived metastable species between two channel segments, which can generate a large local potential and a new breakdown, promoting the occurrence of the short-cutting events between the two channel segments.

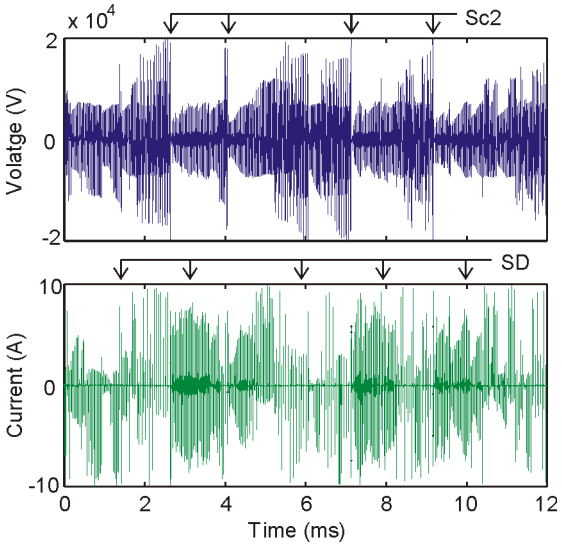

FIG. 16. *Voltage and current waveforms of a gliding arc discharge at 600 W and 42 SLM, showing more frequent transitions among different types of discharges than at a lower flow rate shown in figure 13. Typical examples of discharge phenomena are labeled (SD: spark-type discharges; Sc2: short-cutting between two electrodes).*

Table. 1 The Reynolds number and the Kolmogorov length of the turbulent flows

V (SLM)	*v(m/s)*	*Re*	*η (μm)*
17.5	*41*	*8000*	*851*
42	*99*	*19200*	*60*

V is the air flow rate. v is the exit velocity of the jet nozzle. Re is the Reynolds number. η is the Kolmogorov length.

C. Effect of input powers

Figure 17 shows the voltage and current waveforms at 17.5 SLM and 800 W. This corresponds to the operating condition for the gliding arc discharge in figure 1(c). In figure 17, few transitions among different types of discharges that are represented by current spikes can be seen. The sustained glow-type discharge dominates during the time span observed. It seems that a relatively high power could suppress transitions among different types of discharges. Too low input power is not sufficient to sustain the plasma column which is cooled and transported by the turbulent air flow, and the plasma column is more likely to fade away and the impedance increases. This leads to an increase of the potential and results in more frequent transitions among different types of discharges. Thus, a moderate input power is able to generate a sustained diffusive glow-type discharge stabilized at about 0.2 *A* at a flow rate of 17.5 SLM by which a non-thermal state can be achieved[27].

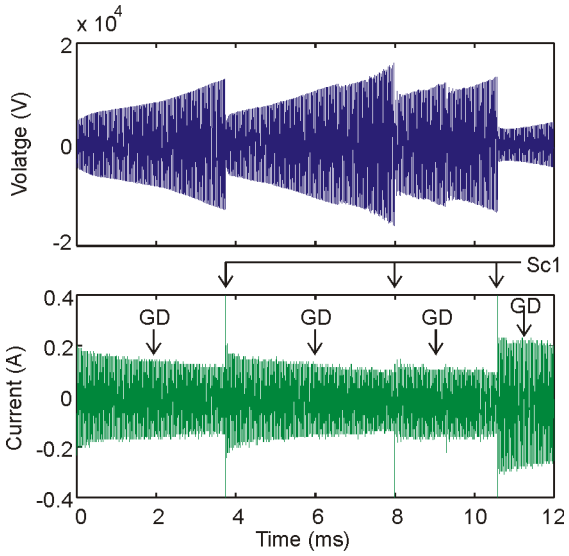

FIG. 17. *Voltage and current waveforms of a gliding arc discharge at at 800 W and 17.5 SLM, showing less frequent transitions among different types of discharges than at a lower input power shown in figure 13. Typical examples of discharge phenomena are labeled (GD: glow-type discharge; Sc1: short-cutting between two channel segments).*

Figure 18 summarizes peak voltage per unit length (PVPL) for the glow-type discharges, the spark-type discharges, and transitions between them with different input powers at 17.5 SLM. The PVPL for initiating the spark-type discharge at 600 W is 120 kV/m whereas the PVPL for the glow-type discharge is 89 kV/m. For a shorter plasma column, e.g. a 4 cm plasma column shown in figure 7(b), the required voltage for initiating the spark discharge is less than 5 kV, which is achieved with a period of 14 μs since the voltage recovery rate is 350 V/μs. However, when the plasma column becomes longer, e.g. a 15 cm plasma column shown in figure 11(b), the peak voltage for initiating the spark discharge is about 18.7 kV, which requires around 84 μs for the peak voltage to recover to 18.7 kV since the voltage recovery rate is about 220 V/μs.

At 600 W, the PVPL for the spark-type and glow-type discharges is close, which suggests that transitions between these two types of discharges are easier, as shown in figure 13 and figure 18. When the input power is increased to 800 W, the PVPL becomes 70 kV/m, which is much smaller than the value for initiating the spark-type discharge. In this case, transitions between these two types of discharges rarely occur. If the input power further increases to 1200 W, the PVPL (40 kV/m) of the discharge is far from the regime of the spark-type discharge, and therefore a glow-type discharge can be sustained. Apart from the voltage recovery rate, the occurrence of the spark-type discharge may also be due to the interaction between the residual species and turbulence. Residual long-lived metastable species produced in the previous plasma column may promote the formation of the next bright plasma column with a current spike in the previous channel. However, on the other hand, the turbulent flow enhances the heat and mass transfer and prevents accumulations of the residual metastable species.

The alternately bright and dark fringes of the plasma columns in figure 1(a) and 1(b) are due to occurrence of the spark-type discharge. The spark-type discharge is characterized by a transient bright plasma column, cf. figure 9 (b), and the time interval for the spark discharge with a long plasma column is up to 70 or 84 μs. The speed of the plasma column at 17.5 SLM was reported to be 8 m/s [14]. During the time span of 70 or 84 μs, the plasma column can travel a distance of about 0.5 - 0.7 mm, which agrees well with the marked traveling distance in figure 1(a). For the plasma column at 42 SLM, the plasma column moves faster, and therefore it shows a longer traveling distance as marked in figure 1(b). In figure 1(a), much less bright plasma columns are observed than figure 1(b), showing agreement with the fact that less current spikes occur in fig-

ure 13 than those shown in figure 16. Besides, the frequent re-ignitions at 42 SLM make it easier to capture the re-ignition event with a digital camera, cf. figure 1(b). By operating the gliding arc discharge at a higher power, the discharge imaged in figure 1(c) shows no indications of bright plasma column, which is also supported by figure 17 where the current spike is rarely seen.

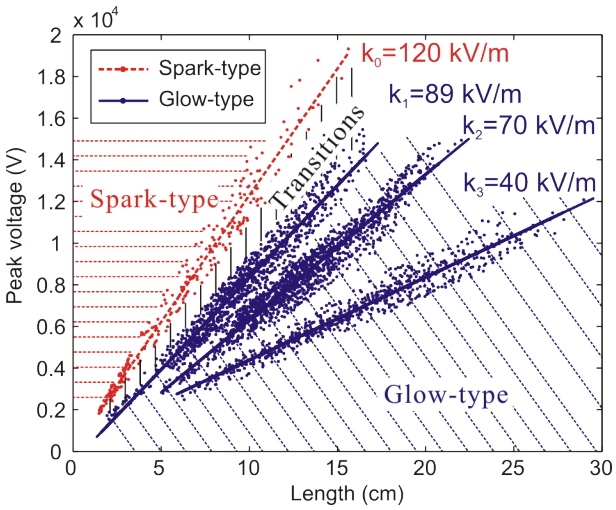

FIG. 18. *Spark-type discharges, glow-type discharges and their transitions distinguished by Peak voltage per unit length (PVPL) for initiating the discharges at 17.5 SLM. The slope k_0 is the PVPL for initiating the spark-type discharge at 600 W while the slope k_1, k_2 and k_3 represents the PVPL for the glow-type discharge at 600 W, 800 W and 1200 W, respectively.*

V. SUMMARY

In summary, spatiotemporally resolved characteristics of a 35 kHz AC gliding arc discharge generated in a turbulent air flow at atmopheric pressure were studied using simultaneously optical and electrical diagnostics. Instantaneous images of plasma columns were taken at a frame rate of up to 480 kHz, with the voltage and current waveforms simultaneously recorded. In particular, detailed imaging and analysis of short-cutting phenomena and transitions among different types of discharges were presented.

Three different types of short-cutting phenomena were recognized, and the short-cutting events can enable the short-cut upper part of the plasma column to fade away in hundreds of microsecond without current passing through it, which suggests the existence of residual long-lived metastable species.

Transitions among glow-type discharges, spark-type discharges and short-cutting events were observed and discussed. The transitions can not only be found to take place from spark-type discharges and glow-type discharges, but also be observed in the opposite way. Short-cutting events were often observed as the intermediate states formed during the spark-glow transitions.

The transitions among different types of discharges are mainly affected by the voltage recovery rate, the period of AC driving signal, the flow rates and the rated input powers. The voltage recovery rate and the period of AC driving signal determines the time interval of two sequential spark-glow transitions. Turbulent effects, such as convective cooling, the twist and wrinkle of plasma columns, and transportation of long-lived metastable species, can significantly affect transitions among the different types of discharge phenomena. With a stonger turbulent flow, the glow-type discharges are more frequently transferred to spark-type discharges. When the input power of the discharge is not sufficient to sustain the plasma column, which are cooled and transported by the turbulent air flow, the plasma column is more likely to fade away and it leads to the formation of more frequent short-cutting events and spark-type discharges.

Further spatiotemporally resolved optical diagnostics of the glow-type discharge, the spark-type discharge and short-cutting phenomena are required to obtain the spectral information and the temperature so as to enrich the undstanding of gas discharge physics and chemistry in a turbulent air flow at amospheric pressure.

Acknowledgments

The work was financially supported by the Swedish Energy Agency, Swedish Research Council (VR), Knut & Alice Wallenberg Foundation, European Research Council and National Natural Science Foundation of China (No. 51606217, 91541203).

References

1.A. Czernichowski, Pure Appl Chem **66** (6), 1301-1310 (1994).
2.A. Fridman, S. Nester, L. A. Kennedy, A. Saveliev and O. Mutaf-Yardimci, Prog Energ Combust **25** (2), 211-231 (1999).
3.J. H. Yan, C. M. Du, X. D. Li, X. D. Sun, M. J. Ni, K. F. Cen and B. Cheron, Plasma Sources Sci T **14** (4), 637-644 (2005).

4.Z. Bo, J. H. Yan, X. D. Li, Y. Chi, K. F. Cen and B. G. Cheron, Plasma Chem Plasma P **27** (5), 546-558 (2007).
5.X. Tu and J. C. Whitehead, Int J Hydrogen Energ **39** (18), 9658-9669 (2014).
6.V. Dalaine, J. M. Cormier and P. Lefaucheux, J Appl Phys **83** (5), 2435-2441 (1998).
7.C. M. Du, J. H. Yan and B. Cheron, Plasma Sources Sci T **16** (4), 791-797 (2007).
8.T. Ombrello, X. Qin, Y. G. Ju and C. Carter, Aiaa J **44** (1), 142-150 (2006).
9.A. Fridman, A. Gutsol, S. Gangoli, Y. G. Ju and T. Ombrellol, J Propul Power **24** (6), 1216-1228 (2008).
10.Y. Kusano, J. J. Zhu, A. Ehn, Z. S. Li, M. Aldén, M. Salewski, F. Leipold, A. Bardenshtein and N. Krebs, Surf. Eng. **31** (4), 282-288 (2015).
11.Y. Kusano, M. Salewski, F. Leipold, J. Zhu, A. Ehn, Z. Li and M. Aldén, Eur Phys J D **68** (10), 319 (2014).
12.Y. Kusano, B. F. Sorensen, T. L. Andersen, H. L. Toftegaard, F. Leipold, M. Salewski, Z. W. Sun, J. J. Zhu, Z. S. Li and M. Aldén, J. Phys. D: Appl. Phys. **46** (13), 135203 (2013).
13.Z. B. Feng, N. Saeki, T. Kuroki, M. Tahara and M. Okubo, Appl Phys Lett **101** (4), 041602 (2012).
14.Z. W. Sun, J. J. Zhu, Z. S. Li, M. Alden, F. Leipold, M. Salewski and Y. Kusano, Opt Express **21** (5), 6028-6044 (2013).
15.J. Zhu, Z. Sun, Z. Li, A. Ehn, M. Alden, M. Salewski, F. Leipold and Y. Kusano, J Phys D Appl Phys **47** (29), 295203 (2014).
16.A. Czernichowski, H. Nassar, A. Ranaivosoloarimanana, A. A. Fridman, M. Simek, K. Musiol, E. Pawelec and L. Dittrichova, Acta Phys Pol A **89** (5-6), 595-603 (1996).
17.X. Tu, L. Yu, J. H. Yan, K. F. Cen and B. G. Cheron, Phys Plasmas **16** (11), 113506 (2009).
18.T. L. Zhao, Y. Xu, Y. H. Song, X. S. Li, J. L. Liu, J. B. Liu and A. M. Zhu, J Phys D Appl Phys **46** (34), 345201 (2013).
19.B. Benstaali, P. Boubert, B. G. Cheron, A. Addou and J. L. Brisset, Plasma Chem Plasma P **22** (4), 553-571 (2002).
20.A. J. Wu, H. Zhang, X. D. Li, S. Y. Lu, C. M. Du and J. H. Yan, IEEE T Plasma Sci **42** (11), 3560-3568 (2014).
21.N. C. Roy, M. G. Hafez and M. R. Talukder, Phys Plasmas **23** (8), 083502 (2016).
22.C. Zhang, T. Shao, J. Y. Xu, H. Ma, L. W. Duan, C. Y. Ren and P. Yan, Ieee T Plasma Sci **40** (11), 2843-2849 (2012).
23.C. Zhang, T. Shao, P. Yan and Y. X. Zhou, Plasma Sources Sci Technol **23** (3) (2014).
24.L. Potočňáková, J. Šperka, P. Zikán, J. J. W. A. v. Loon, J. Beckers and V. Kudrle, Plasma Sources Sci Technol **24** (2), 022002 (2015).
25.Y. D. Korolev, O. B. Frants, V. G. Geyman, N. V. Landl and V. S. Kasyanov, Ieee T Plasma Sci **39** (12), 3319-3325 (2011).
26.Y. D. Korolev, O. B. Frants, N. V. Landl, A. V. Bolotov and V. O. Nekhoroshev, Plasma Sources Sci Technol **23** (5), 054016 (2014).
27.J. Zhu, J. Gao, Z. Li, A. Ehn, M. Aldén, A. Larsson and Y. Kusano, Appl Phys Lett **105** (23), 234102 (2014).
28.J. Zhu, J. Gao, A. Ehn, M. Aldén, Z. Li, D. Moseev, Y. Kusano, M. Salewski, A. Alpers, P. Gritzmann and M. Schwenk, Appl Phys Lett **106** (4), 044101 (2015).
29.F. Richard, J. M. Cormier, S. Pellerin and J. Chapelle, J Appl Phys **79** (5), 2245-2250 (1996).
30.F. Mitsugi, J. Furukawa, T. Ohshima, H. Kawasaki, T. Kawasaki, S. Aoqui and H. D. Stryczewska, Eur Phys J-Appl Phys **61** (2) (2013).
31.J. Šperka, P. Souček, J. W. A. Loon, A. Dowson, C. Schwarz, J. Krause, G. Kroesen and V. Kudrle, Eur. Phys. J. D. **67** (12), 261 (2013).
32.T. L. Zhao, J. L. Liu, X. S. Li, J. B. Liu, Y. H. Song, Y. Xu and A. M. Zhu, Phys Plasmas **21** (5) (2014).
33.S. P. Gangoli, A. F. Gutsol and A. A. Fridman, Plasma Sources Sci Technol **19** (6), 065003 (2010).
34.S. P. Gangoli, A. F. Gutsol and A. A. Fridman, Plasma Sources Sci Technol **19** (6), 065004 (2010).
35.S. Pellerin, J. M. Cormier, F. Richard, K. Musiol and J. Chapelle, Journal of Physics D-Applied Physics **32** (8), 891-897 (1999).
36.S. Pellerin, F. Richard, J. Chapelle, J. M. Cormier and K. Musiol, Journal of Physics D-Applied Physics **33** (19), 2407-2419 (2000).
37.A. Larsson, L. Adelow, M. Elfsberg and T. Hurtig, IEEE T Plasma Sci **42** (10), 3186-3190 (2014).
38.I. V. Kuznetsova, N. Y. Kalashnikov, A. F. Gutsol, A. A. Fridman and L. A. Kennedy, J Appl Phys **92** (8), 4231-4237 (2002).
39.S. Y. Lu, X. M. Sun, X. D. Li, J. H. Yan and C. M. Du, Phys Plasmas **19** (7) (2012).
40.F. Mitsugi, T. Ohshima, H. Kawasaki, T. Kawasaki, S.-I. Aoqui, T. Baba and S. Kinouchi, IEEE T Plasma Sci **42** (12), 3681-3686 (2014).
41.O. Mutaf-Yardimci, A. V. Saveliev, A. A. Fridman and L. A. Kennedy, J Appl Phys **87** (4), 1632-1641 (2000).
42.S. Kolev and A. Bogaerts, Plasma Sources Sci Technol **24** (1), 015025 (2015).